scientific reports

Check for updates

OPEN

Circulating IL6 is involved in the infiltration of M2 macrophages and CD8+T cells

Jing Huang[1,4], Rui Xiao[1,4], Suyujie Shi[1,4], Qingshu Li[1,2,3], Ming Li[1,2,3], Ming Xiao[1,2,3], Yalan Wang[1,2,3], Yaying Yang[1,2,3], Wenwen Li[1,2,3]✉ & Yi Tang[1,2,3]✉

To elucidate the relationship between circulating cytokines and the prognosis of microsatellite-stable(MSS) colorectal cancer (CRC) patients, we examined the correlation between circulating cytokine levels and tumor immune infiltration microenvironment in this patient population. By conducting a preliminary analysis of the GEO database, we identified five core genes associated with colorectal cancer and further analyzed their impact on immune infiltration. We measured serum cytokine levels and validated the immune infiltration results through immunohistochemical staining of common inflammatory cell markers, including CD3, CD4, CD8, CD163, and FOXP3. Our findings indicate that serum cytokine levels significantly influence immune infiltration in colorectal cancer, particularly IL6 and IFNγ, which play crucial roles. Specifically, the infiltration of M2-type macrophages and CD8+T cells is correlated with serum levels of IL6 and IFNγ. MSS CRC patients with elevated IL6 expression exhibit improved prognosis.

The combined analysis of tumor-infiltrating lymphocytes (TIL) and microsatellite instability (MSI) status has consistently guided clinical treatment decisions in colorectal cancer. In patients with MSI CRC, immune checkpoint inhibitors (ICIs) are recommended, while ICIs treatment does not provide significant benefits for 90% of patients with MSS CRC[1–4]. This discrepancy may be attributed to the unique tumor immune microenvironment observed in MSS CRC[5–8]. During the investigation of various cells within the tumor immunosuppressive microenvironment, researchers have identified certain cytokines that play a role in immune infiltration processes. For instance, IL6 is involved in the immune infiltration process of NK cells, Treg cells, and CD8+T cells[9–12]. However, most studies have focused on cytokine levels within cells and their immediate surroundings only[13]. Few researchers studying solid tumors have explored the role of cytokines present in serum samples. However, serum levels of cytokines can influence tumor therapy and can also be used as predictors of treatment response[14,15]. Malignant tumors are systemic diseases. Therefore, the significance of circulating components in tumorigenesis and progression becomes evident under this perspective. Notably, targeted cytokine therapies directly enter circulation as a primary route during treatment administration. Studies conducted on colorectal cancer and pancreatic cancer have demonstrated a close association between serum levels of cytokines such as IL6 and overall patient survival rates[16,17].Serum IL6 testing has also revealed an association between its levels and diffuse large B cell lymphoma (DLBCL) occurrence[18]. There is limited research on the relationship between serum cytokines and the immune infiltration microenvironment in patients, and it remains unclear whether common serum cytokine levels influence patient prognosis by altering the tumor immune infiltration.

We hypothesized that serum levels of common cytokines may impact the prognosis of patients with MSS CRC by modifying the immune infiltration microenvironment. To investigate this hypothesis, we screened three gene expression datasets from the GEO database, extracting 1893 genes for differential expression analysis. Subsequently, WGCNA analysis yielded 19 co-expression modules, from which 1301 key genes were selected for GO/KEGG analysis and PPI network construction. Ultimately, we identified 10 key genes. Special attention was given to IL-6, IFNG, and IL-2 to explore their potential correlations with immune cell infiltration patterns. Immunohistochemical staining was employed to assess the expression of common tumor-associated immune cells (CD3, CD4, CD8, CD163, and FOXP3), while flow cytometry measured serum cytokine levels. Statistical results indicate that IL-6 is one of the most significant serum cytokines influencing the prognosis of MSS CRC patients by participating in immune infiltration processes. IL-6 is closely associated with M2-type macrophage and CD8+T cell infiltration. Serum IFNγ correlates with M2 macrophage and CD4+T cell infiltration.

[1]Department of Pathology, College of Basic Medicine, Chongqing Medical University, Chongqing, China. [2]Molecular Medicine Diagnostic and Testing Center, Chongqing Medical University, Chongqing, China. [3]Department of Pathology, The First Affiliated Hospital of Chongqing Medical University, Chongqing, China. [4] Jing Huang, Rui Xiao and Suyujie Shi contributed equally to this work. ✉email: liwenwen@cqmu.edu.cn; 102785@cqmu.edu.cn

The collective levels of serum cytokines jointly influence immune cell infiltration in the MSS CRC tumor microenvironment. There may be synergistic or antagonistic interactions between cytokines, contributing to the poor immune microenvironment in MSS CRC through complex mechanisms. Notably, IL-6 and IFNγ may play a role in developing immune resistance in MSS CRC.

Results

Identification of differentially expressed and modular genes

As illustrated in Fig. 1A,B, a total of 1,893 differentially expressed genes (DEGs) were identified between the tumor and control groups following batch effect correction of the datasets GSE35279, GSE87211, and GSE110224. As depicted in Figs. 1D, amp and E and 880 genes were upregulated while 1,013 genes were downregulated. Weighted gene co-expression network analysis (WGCNA) was employed to identify gene modules associated with CRC. As shown in Fig. 2A,B, an R-squared value greater than 0.8 determined that a soft threshold power of 4 was optimal. After merging similar modules, a total of 19 distinct modules were identified and visualized through a cluster dendrogram (Fig. 2C). In the heatmap illustrating the module-clinical trait relationship, the turquoise module exhibited the strongest correlation with the tumor clinical trait ($r = 0.33$) (Fig. 2D). In Fig. 2E, the average gene significance within each module is presented. Subsequently, we constructed a correlation plot between module members and gene significance for the turquoise module, resulting in the identification of 5,980 genes (correlation coefficient = 0.94, P-value = 1e-200) (Fig. 2F). The study procedures are shown in the (Fig. 1C).

GO and KEGG enrichment analyses

As illustrated in Fig. 2, the intersection of genes selected through Weighted Gene Co-expression Network Analysis (WGCNA) and differentially expressed genes (DEGs) resulted in a total of 1301 overlapping genes. These genes were identified as candidate genes that are likely to play crucial roles in the development and progression of colorectal cancer (Fig. 2G). To further elucidate their potential functions, Gene Ontology (GO) and Kyoto Encyclopedia of Genes and Genomes (KEGG) pathway analyses were conducted[19–21]. A total of 20 pathway terms were identified, with the top 10 pathways visualized in a bubble plot ranked by p-value (Fig. 2I) and detailed in Supplementary Table S1. KEGG enrichment analysis revealed that these genes were primarily involved in pathways such as "Cytokine-cytokine receptor interaction," "Neuroactive ligand-receptor interaction," "Viral protein interaction with cytokine and cytokine receptor," "IL-17 signaling pathway," and "Calcium signaling pathway." Following GO analysis using the R package, a total of 792 GO terms were obtained, comprising 630 Biological Process (BP) terms, 41 cellular component (CC) terms, and 121 Molecular Function (MF) terms. The top six BP, CC, and MF terms with the lowest p-values are depicted in circular plots (Fig. 2H) and summarized in Supplementary Table S2. Key BP terms included "inorganic anion transport," "hormone metabolic process," "chloride transport," "monoatomic anion transport," and "vascular process in circulatory system." CC terms mainly encompassed "apical plasma membrane," "apical part of cell," "basal plasma membrane," "basal part of cell," and "basolateral plasma membrane." MF terms predominantly covered "cytokine activity," "growth factor activity," "monoatomic ion channel activity," "chloride transmembrane transporter activity," and "inorganic anion transmembrane transporter activity."

PPI network analysis and hub gene identification

To identify hub genes, we analyzed 1301 intersection genes using the STRING online platform, setting the confidence level to the highest (0.9) and concealing unconnected nodes to construct a protein-protein interaction (PPI) network (Fig. 2J). Subsequently, the degree values were calculated using the cytoHubba plugin in Cytoscape software. Nodes were ranked based on their degree, with node size and color intensity positively correlated with the degree ranking. This process identified 10 hub genes: IL6, CXCL10, PRKACB, IFNG, IL1A, CXCL2, IL2, CXCL1, AGT, and CSF2 (Fig. 2K). The corresponding degree values are provided in Supplementary Table S3.

ROC curve and clinical prediction model construction of related genes

The Receiver Operating Characteristic (ROC) curves of the top five hub genes were computed to assess their diagnostic performance. The Area Under the Curve (AUC) for all hub genes exceeded 0.7, indicating a satisfactory model fit (Fig. 3A,B). The hub genes identified were CXCL10, IL6, PRKACB, IFNG, and IL1A. A total score was derived by assigning each gene a score based on its value on the point scale axis, summing these individual scores, and projecting the result onto a lower total score scale to estimate the risk of colorectal cancer (Fig. 3A,B). Overall, the model demonstrated robust predictive performance. The Mean Absolute Error (MAE = 0.03) and Mean Squared Error (MSE = 0.00138) were minimal, suggesting that the model provided relatively accurate predictions in most instances. The 0.9 quantile of the absolute error was 0.068, indicating that the prediction error did not exceed 0.068 in 90% of cases, further validating the model's reliability. The calibration curve of the nomogram (Fig. 3C) showed high concordance between the predicted and actual probabilities of colorectal cancer. Analysis of the GSE44076 validation set revealed significant differences in expression levels of the top five hub genes between the tumor and control groups (Fig. 3D). With the exception of IFNG, the AUC values for the other four hub genes exceeded 0.7 (Fig. 3E).

Immune infiltration and its association with hub genes

The immune infiltration of hub genes, which are clinically common indicators including IL6, IL2, and IFNG, was analyzed. Additionally, the CIBERSORT algorithm was employed to further elucidate the disparities in the immune microenvironment. Figure 4A depicts the ratio of 22 immune cells between the tumor and control groups. A correlation matrix was constructed to identify robust positive or negative associations among different types of immune cells (Fig. 4B). Then, the differences of 22 immune cell infiltration in tumor and normal tissues

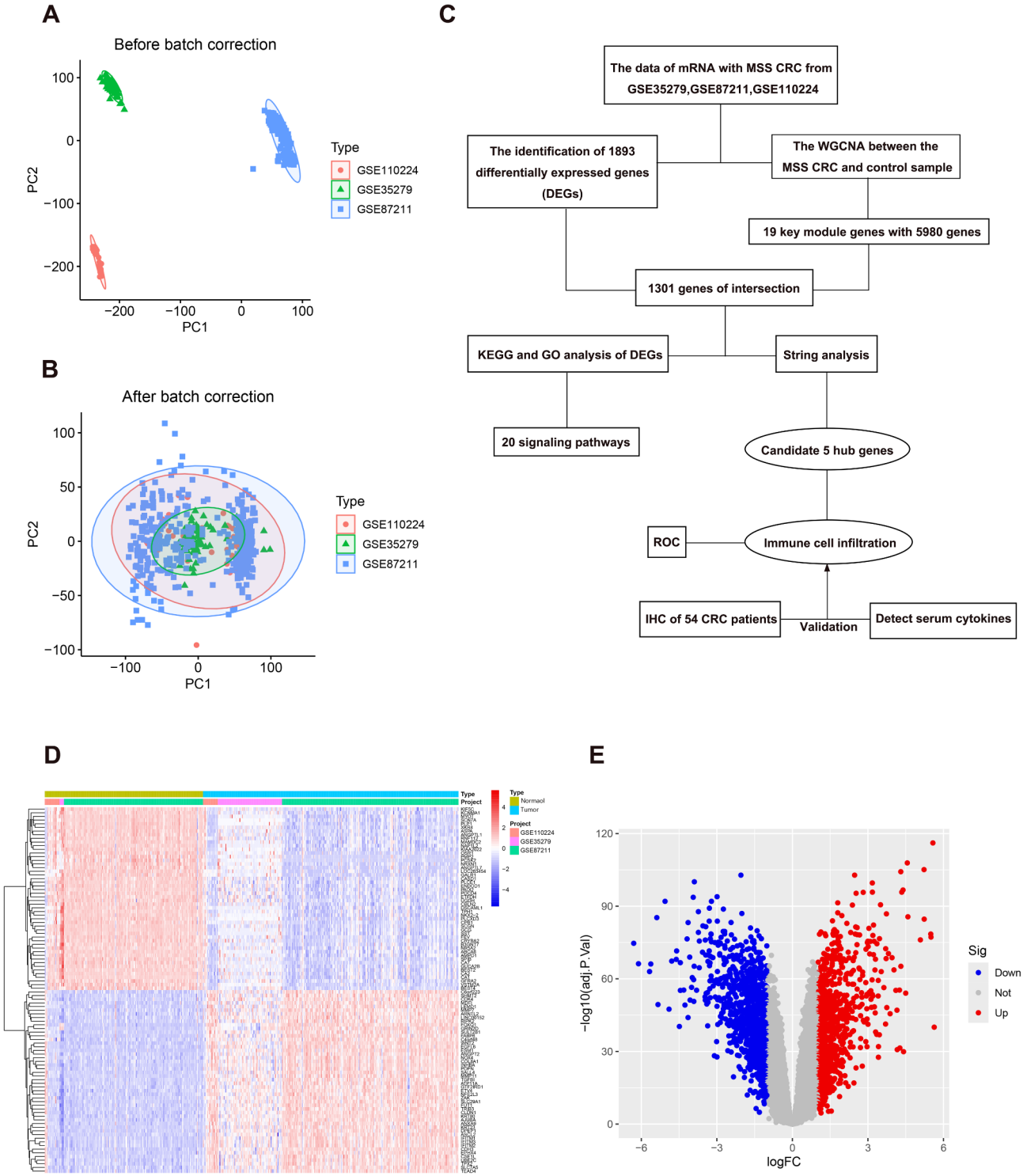

Fig. 1. Principal component analysis (PCA) and the differential gene expression in colorectal cancer. (**A**) PCA analysis was conducted to identify pre-batch effects. (**B**) After removing the batch effect, PCA analysis was performed again, using principal components 1 (PC1) and 2 (PC2) as x- and y-axes respectively, to generate scatter plots where each point represents a sample. The greater the distance between two samples, the more distinct their gene expression patterns are. (**C**) The study flow chart is presented for reference. (**D**) A heat map of differentially expressed genes (DEGs) between tumor group and control group is shown, with color gradient ranging from blue to red indicating down-regulation to up-regulation in expression levels; color intensity reflects z-score normalized expression values. (**E**) A volcano map displays DEGs between tumor group and control group, with up-regulated genes represented by red dots, down-regulated genes by blue dots, and genes without significant changes in expression shown as gray dots.

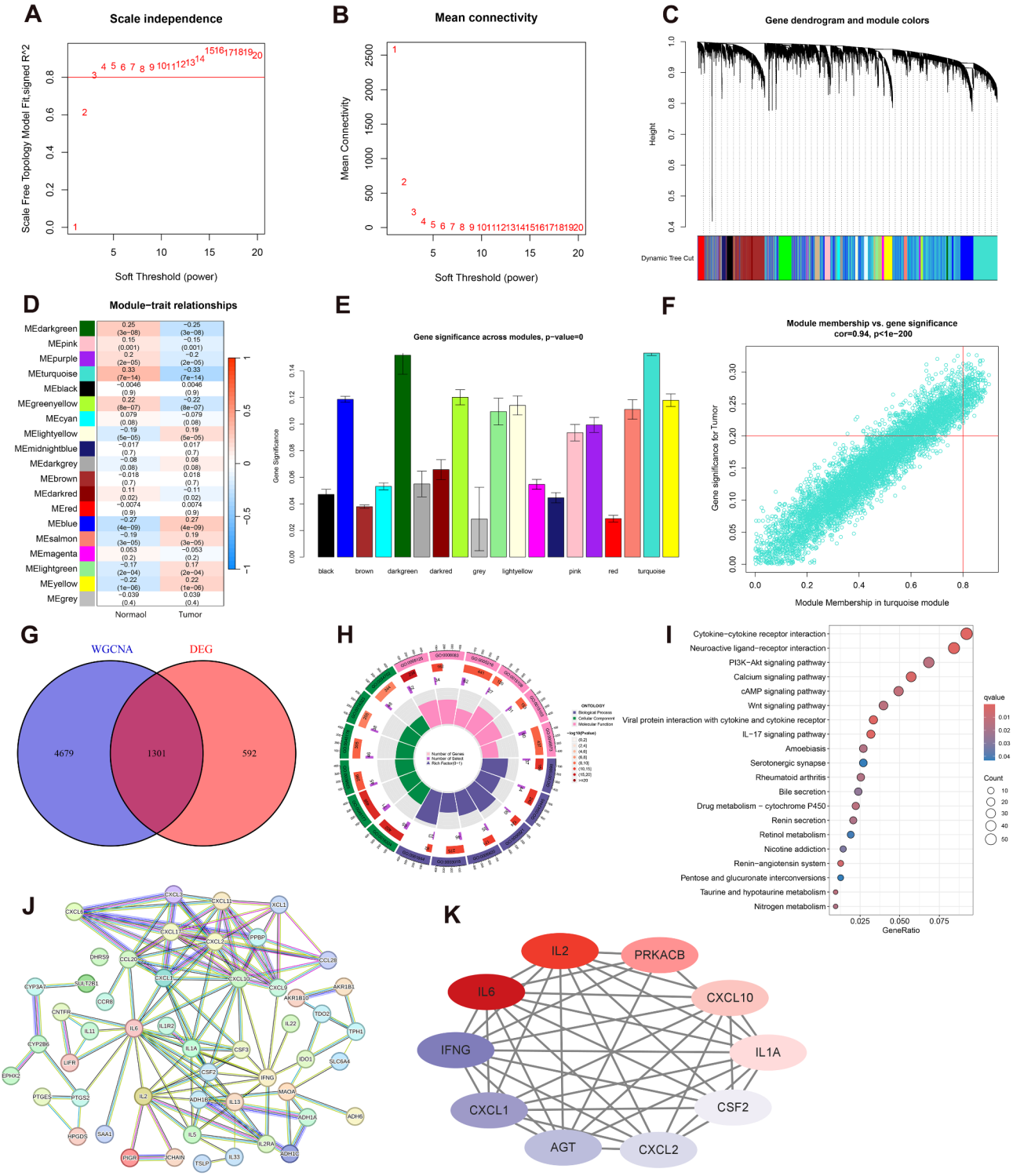

Fig. 2. GO/KEGG enrichment analysis, PPI network construction, and hub gene identification were conducted. (**A**,**B**) Determine the optimal soft threshold for the dataset. (**C**) Gene co-expression modules indicated in different colors under the cluster tree. (**D**) Identify modules that are highly correlated between the tumor group and healthy controls. (**E**) Distribution of mean gene significance in each module. (**F**) Correlation plot between module membership and gene significance of genes included in the turquoise module. (**G**) Venn diagram showing 1301 overlapping candidate core genes. (**H**) GO enrichment analysis of core genes. (**I**) KEGG pathway analysis of core genes. (**J**) PPI network visualization highlights interactions between proteins encoded by intersection genes. (**K**) The core genes of the interaction network are obtained by the degree centrality algorithm. (K) ROC curves depicting the performance of the top five hub genes.

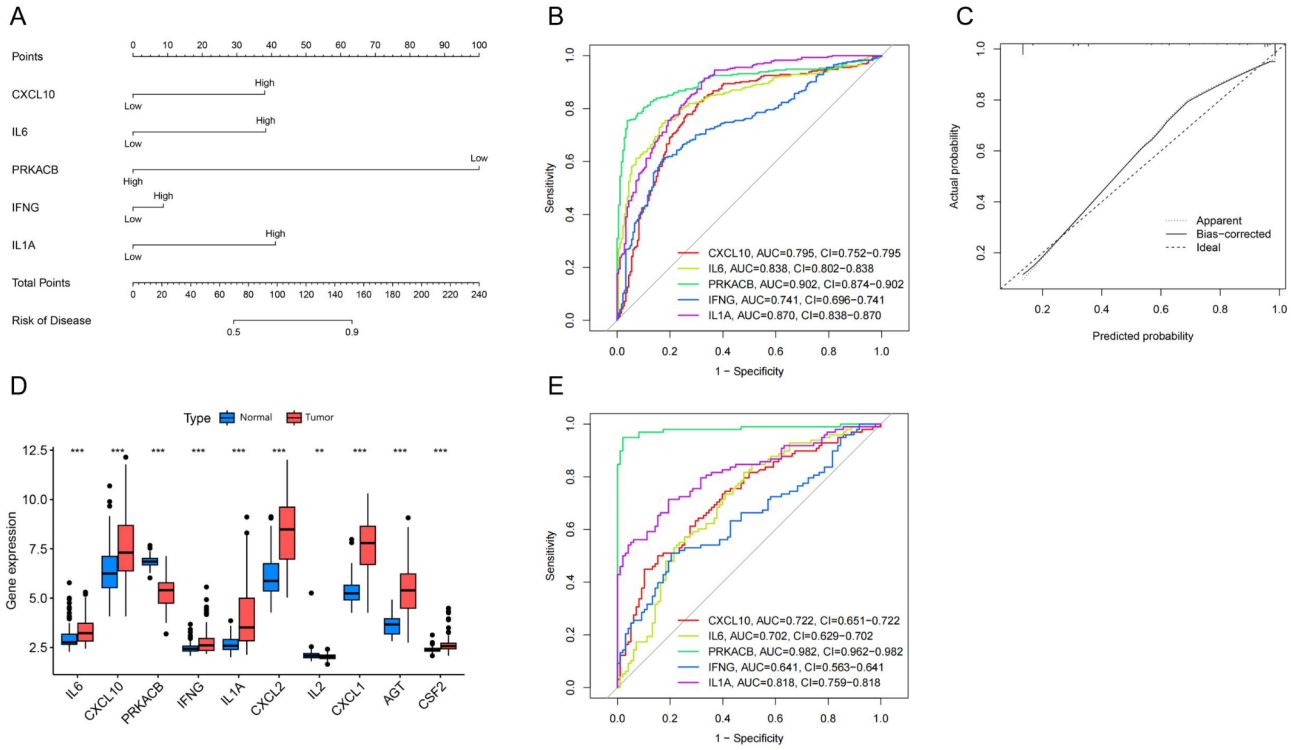

Fig. 3. Construction and evaluation of ROC curves and a clinical prediction model for related genes. (**A**) Development of a nomogram to predict the risk of colorectal cancer. (**B**) ROC curves for the top five hub genes. (**C**) Calibration curve for the nomogram. (**D**) Boxplots illustrating the expression levels of hub genes in the tumor versus control groups within the validation cohort. (**E**) ROC curve for validating diagnostic performance in the validation set.

were analyzed (Fig. 4D). In comparison with the control group, higher proportions of Plasma cells, T cells CD8, T cells CD4 naive, T cells CD4 memory resting, T cells CD4 memory activated, regulatory T-cells (Tregs), NK cells resting Macrophages M0 Dendritic Cells activated and Mast Cells activated were observed in the tumor group. Conversely B-cells naive B-cells memory follicular helper T-cells Monocytes Macrophages M2 Mast Cells resting Neutrophils exhibited relatively lower proportions in both groups ($p < 0.05$).

To further investigate the potential association between the expression of key genes IL-6, IFNG, and IL-2 and patterns of immune cell infiltration(Fig. 5A), we presented a lollipop plot (Fig. 4D-F) to demonstrate the Spearman correlation between the expression of these three key genes and immune cell enrichment. Among these, IL-6 exhibited a positive correlation with neutrophils, activated mast cells, monocytes, and CD4 naive T cells. This indicates that the infiltration of these immune cells in the tumor microenvironment may increase as IL-6 expression levels rise. The positive correlation suggests that IL-6 may play a regulatory role in the function and distribution of these immune cells. Conversely, IL-6 showed a negative correlation with M2-type macrophages, CD8 T cells, M1-type macrophages, and naive B cells, implying that elevated IL-6 expression levels may reduce the infiltration of these immune cells. This negative correlation reflects both the inhibitory effects of IL-6 on various immune cell types and the presence of complex mutual regulatory mechanisms between these immune cells and IL-6. The identical trend was also evident in the GSE44076 validation set (see Supplementary Fig. 1). Additionally, IFNG demonstrated a negative correlation with Tregs, resting CD4 memory T cells, resting NK cells, and naive B cells, while showing a positive correlation with activated CD4 memory T cells, activated NK cells, and dendritic cells. IL-2 was negatively correlated with resting NK cells, neutrophils, and monocytes, but positively correlated with M2 macrophages and CD8 T cells.

Notably, the infiltration of M2 macrophages and CD8 + T cells exhibited significant correlations with the levels of IL-6 and IL-2. Specifically, M2 macrophage and CD8 + T cell infiltration showed a negative correlation with IL-6 levels but a positive correlation with IL-2 levels. In the validation cohort, the significant impact of IL-6 on M2 macrophage infiltration was similarly confirmed (Supplementary Fig. 1). Additionally, we observed that IL-6 and IFN-γ predominantly influenced the infiltration of CD4 + T cells. The distinction between the two groups was that IFN-γ primarily affected the infiltration of memory CD4 + T cells, while IL-6 mainly influenced naive CD4 + T cells. Elevated IFN-γ levels were associated with increased infiltration of activated memory CD4 + T cells, whereas reduced IFN-γ levels correlated with another subset of CD4 + T cells.

The protein-protein interaction network indicated a significant association between IL6, IL2, IFNG, and other cytokines (Fig. 5B). We conducted an enrichment analysis using the TCGA database for genes related to IL6, IL2, IFNG, CD163, CD8, and CD4. KEGG pathway analysis revealed that cytokines such as IL6 and IL2 are involved in STAT-related signaling pathways. These pathways may play a role in regulating the infiltration of M2

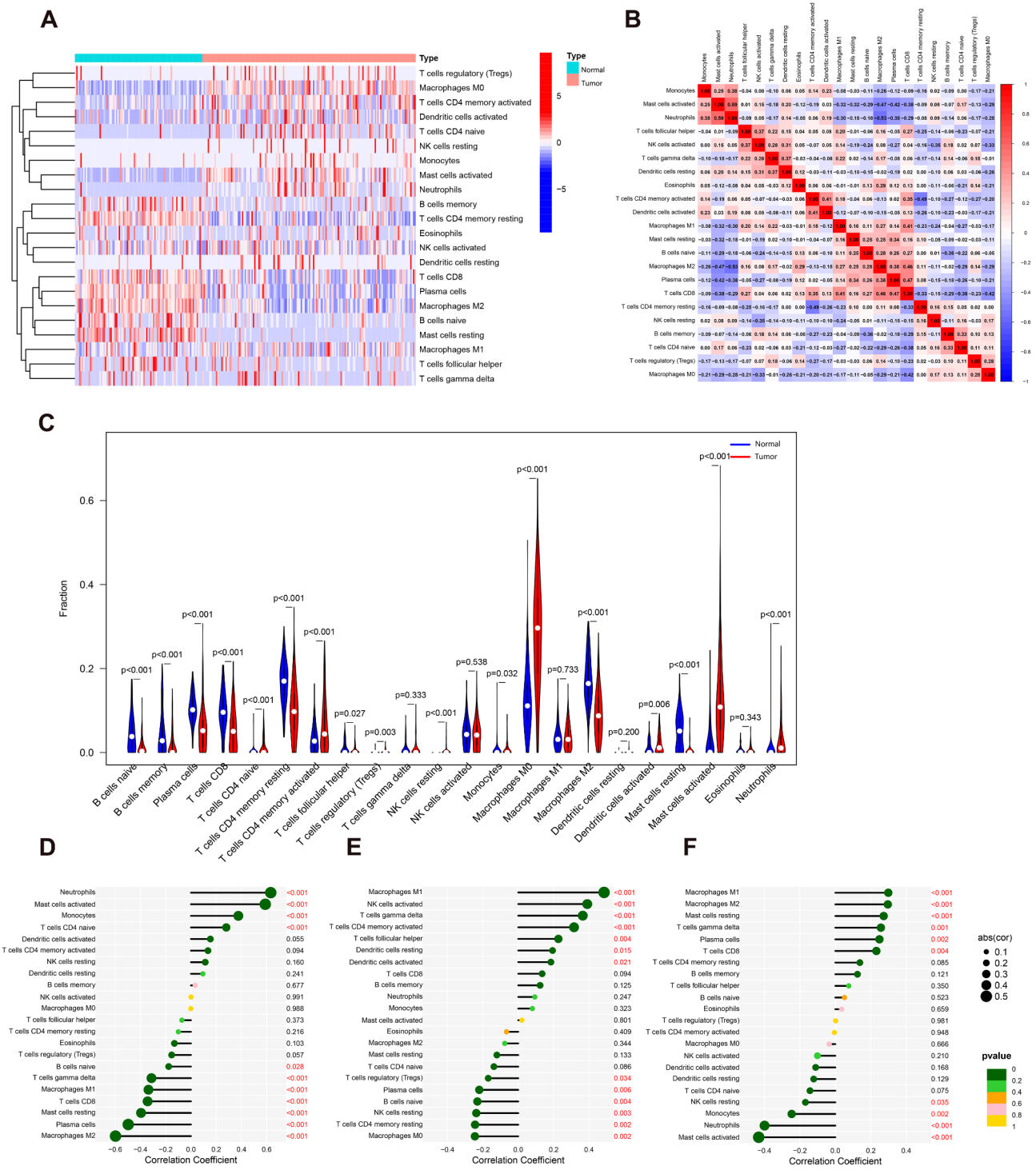

Fig. 4. Analysis of immune cell infiltration. (**A**) Proportions of 22 immune cell subsets between the two groups. (**B**) Correlation analysis of the composition of the 22 immune cell types. (**C**) Comparison of differences in infiltration levels among the 22 immune cell subsets. (**D**) Correlation analysis between IL-6 expression and enrichment levels of immune cells. (**E**) Correlation analysis between IFNG expression and enrichment levels of immune cells. (**F**) Relationship between IL-2 expression and enrichment levels of immune cells.

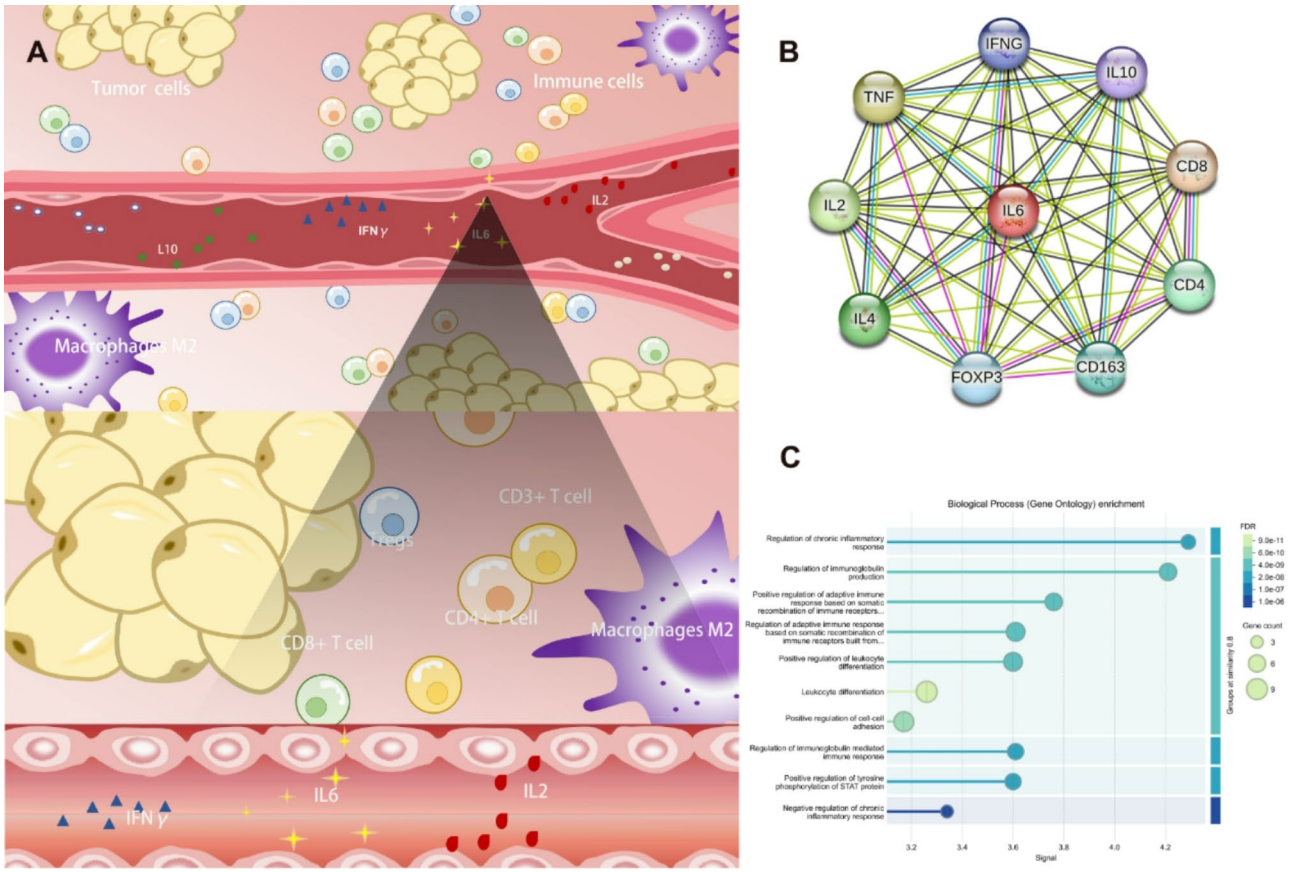

Fig. 5. The interaction between inflammatory cells and cytokines. (**A**) Interaction pattern between blood cytokines and components of tumor immune microenvironment. (**B**) PPI network between inflammatory markers and serum cytokine related genes (from String database). (**C**) The STRING database was utilized to enrich signaling pathways associated with IL6, IL2, IFNG, as well as CD4, CD8, and CD163. These pathways may be linked to inflammatory cell infiltration.

macrophages and CD4 + T cells by IL6, IFNG, and IL2 (Fig. 5C). Therefore, IL-6, IFN-γ, and IL-2 collectively influence the formation of the immune infiltration microenvironment in MSS CRC.

Relationship between immune markers and levels of cytokines in serum

The common inflammatory cell markers (CD3, CD4, CD8, CD163, FOXP3) were immunohistochemically labeled and then the tumor and its surrounding immune-infiltrated areas were divided into intratumoral (T: inside tumor) and tumor invasive front (Q: tumor invasive front) regions for analysis (Fig. 6A). The inflammatory cells in these regions were analyzed along with the corresponding patients' serum cytokine levels. We observed a correlation between certain inflammatory cells and cytokines in the serum (Fig. 6E,F). In terms of spatial distribution, we found a positive correlation between cytokine presence in tumor cells and immune infiltration (Fig. 6F), while there was a negative correlation between invasion front and immune infiltration (Fig. 6E). Furthermore, circulating cytokines exhibited a robust correlation with the infiltration of CD8 + T cells, FOXP3 + Tregs at the tumor invasion front, and CD4 + T cells within the tumor microenvironment. Specifically, the infiltration of CD8 + T cells at the invasion front was inversely correlated with blood levels of IL-2, IL-4, IL-6, and IL-10. Upon stratification by individual cytokine levels, a significant difference in CD8 + T cell infiltration at the invasion front was observed exclusively between groups with varying blood IL-6 level (Fig. 6B). Therefore, the circulating level of IL-6 emerges as a critical determinant influencing CD8 + T cell infiltration at the invasion front. In contrast, the infiltration of CD4 + T cells at the invasion front demonstrated only a weak association with circulating cytokines, whereas intratumoral CD4 + T cells were positively correlated with IL-2, IL-4, TNF-α, and IFN-γ. Further analysis revealed significant differences in intratumoral CD4 + T cell infiltration between groups with different levels of IL-4 and IL-10 (Fig. 6C,D). Consequently, IL-4 and IL-10 collectively play a pivotal role in modulating CD4 + T cell infiltration within the tumor. Additionally, FOXP3 + Tregs at the invasion front exhibited an inverse relationship with IL-2 and IFN-γ. Overall, circulating cytokines predominantly influence the infiltration of CD8 + T cells at the invasion front, with IL-6 being a key factor, while intratumoral CD4 + T cells are primarily regulated by IL-4 and IL-10.

Circulating cytokines exhibited predominantly positive correlations with the infiltration of M2 macrophages (Fig. 6E,F). Specifically, the levels of IL6, TNFα, and IFNγ were positively correlated with the infiltration of

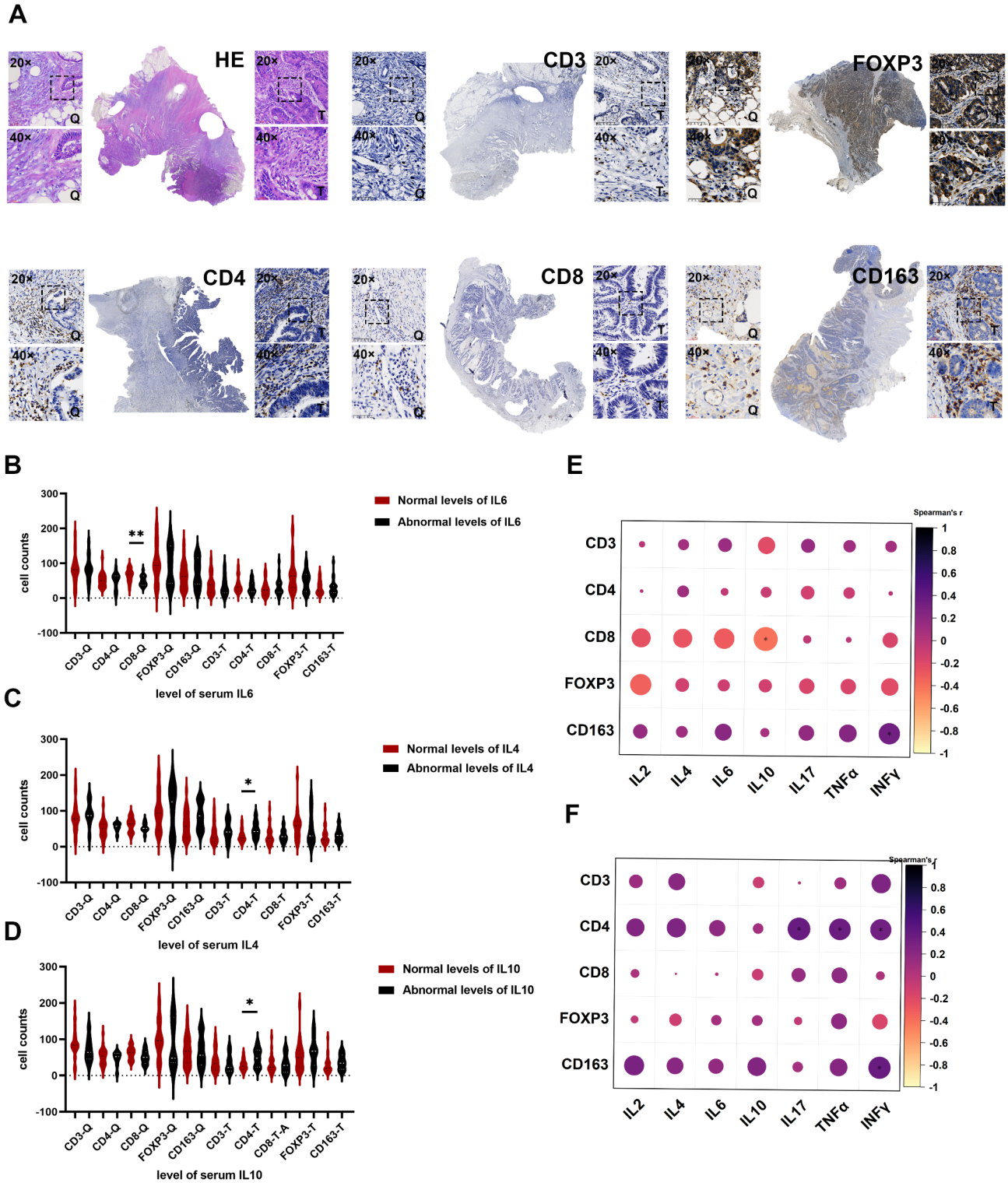

Fig. 6. Association of IHC labeled common cell markers with serum cytokines. (**A**) Immunohistochemical staining was used to identify common tumor-associated inflammatory cells, including CD3, CD4, CD8, CD163, FOXP3, etc., which were further categorized into T (inside the tumor) and Q (tumor invasive front). (**B**) Significant differences were observed in the CD8 + T cell populations at the invasion frontier between groups characterized by abnormal versus normal serum IL-6 levels. (**C**,**D**) Significant differences in the levels of CD4 + T cells within the tumor were observed based on whether the serum concentrations of IL-4 and IL-10 were abnormal. (**E**) The relevance between inflammatory cells within the colorectal tumor invasion front and serum levels of cytokines (IL2, IL4, IL6, IL10 IL17 TNF alpha INF gamma) was examined. (**F**) Correlations between inflammatory cells and serum cytokines within colorectal cancer tumors were analyzed.

M2 macrophages. Additionally, within the tumor microenvironment, the levels of IL2 and IL10 also showed positive correlations with M2 macrophage infiltration. Our findings indicate that both IFNγ and TNFα play crucial roles in M2 macrophage infiltration, whether at the invasive front or within the tumor. Notably, M2 macrophage infiltration at the invasive front is influenced by IL6 levels, whereas within the tumor, both IL2 and IL10 contribute to this process.

Survival analysis pertaining to serum indicators in the MSS CRC cohort

Survival analysis related to serum indicators in the MSS CRC cohort was conducted using KM-ploter, involving 1061 CRC patients (Fig. 7A). The results of survival analysis revealed significant differences in prognosis among CRC patients with varying expression levels of IL6, IFNG, and IL2. Based on the existing CRC guidelines, ICIs were recommended for MSI-H/MMR patients. Subsequently, we stratified the patients into MSS/MSI-L (602 cases) and MSI-H (252 cases) groups and analyzed their cytofactor-related survival separately (Fig. 7B,C). Interestingly, no significant difference in prognosis was observed between MSI-H patients with different cytokine expression levels. However, among MSS/MSI-L patients, although there was no notable disparity in patient prognosis between the IL2 and IFNG groups, it was discovered that MSS/MSI-L CRC patients with a high expression level of IL6 exhibited a better prognosis.

Disscusion

With the extensive exploration of the tumor immune microenvironment, numerous studies have emerged focusing on cytokines within this milieu[22]. In recent years, it has been discovered that targeting IL6 cytokine or combining it with other drugs may effectively enhance the immune microenvironment and ameliorate immunotherapy drug resistance[23]. Additionally, in preclinical models, combined blockade of PD-L1 and IL-6 receptor (IL6R) resulted in synergistic regression of established large tumors and significantly improved antitumor CD8 + cytotoxic T lymphocyte (CTL) responses compared to anti-PD-L1 treatment alone[24]. Hence, immunotherapy and targeted cytokines could potentially serve as effective approaches to enhance patient efficacy and mitigate drug resistance. This is likely due to the association between IL6 and immune infiltration within the environment[25]. However, despite a substantial number of previous studies exploring cytokines within this context, significant breakthroughs are still lacking. It is known that each chemotherapy drug initially enters circulation upon entering the body. Therefore, by observing circulating levels of cytokines alongside immune infiltration in the microenvironment, we aim to provide novel insights into characterizing immune-related characteristics specific to MSS CRC.

To investigate the relationship between serum cytokines and immune infiltration in colorectal cancer (CRC), we utilized the GEO dataset for hub gene identification and analysis of immune infiltration. Ultimately, we identified five hub genes and determined that IL6, IFNG and IL2 were associated with common immune cell infiltration. The infiltration of M2 macrophages and CD8 + T cells was significantly associated with the levels of IL-6 and IL-2, whereas the infiltration of CD4 + T cells was predominantly influenced by both IL-6 and IFN-γ. Subsequently, immunohistochemical labeling was performed on colorectal cancer samples from 55 patients to partition tumor tissue and record the levels of multiple cytokines in their blood. Immunohistochemical analysis confirmed the influence of IL-6 and IL-2 on the infiltration of CD8 + T cells and M2 macrophages. In contrast, IL-4 and IL-10 were identified as the primary cytokines affecting the infiltration of CD4 + T cells in human tissues. Additionally, survival analysis was conducted for microsatellite stable (MSS) colorectal cancer (CRC). Among MSS/MSI-L patients, those with high expression levels of IL-6 exhibited a better prognosis. However, survival analyses of IL-2 and IFN-γ did not indicate a significant impact on patient outcomes. Therefore, while IL-6, IL-2, and IFN-γ collectively contribute to the formation of the immune infiltration microenvironment in MSS CRC, IL-6 remains the predominant prognostic factor. Our findings suggest that detecting serum-related cytokines in clinical practice may serve as an important tool for evaluating patient prognosis. Furthermore, cytokines such as IL-6 have the potential to become critical biomarkers for the diagnosis and treatment of colorectal cancer. Targeting IL-6 and other associated cytokines may also significantly influence patient outcomes.

Interleukin-6 (IL6) is a pleiotropic cytokine that plays a crucial role in regulating the immune system. Numerous preclinical and clinical studies have elucidated the pathological roles of IL-6 in inflammation, autoimmunity, and malignancy. Moreover, the IL-6 related pathway has been implicated in the development and progression of colorectal cancer[26–28],efficacy and drug resistance[29], as well as metastasis[30]. There is indeed a discernible disparity in serum IL6 levels between colorectal cancer patients and normal groups[31]. Previously, IL6 has been demonstrated to modulate Th17 and Treg cells while being localized at sites of macrophage infiltration[32,33]. In another study conducted by Chen Wei et al., co-culturing CRC cells with M2 macrophages revealed that IL6 was an indispensable component of EMT induced by tumor-associated macrophages in CRC[12]. Although these studies primarily focused on tumor-localized IL6, we also discovered a correlation between serum IL6 levels and M2 macrophages, underscoring the significant relevance of circulating cytokine levels for tumorigenesis. IL6 plays a crucial role in the activation of TAMs and their polarization towards the M2 phenotype[34]. Therefore, we hypothesize that the elevated levels of IL6 observed in M2 macrophage infiltration may be attributed to its pro-polarizing effect.

In addition to the role of circulating IL-6 in the tumor microenvironment, we hypothesize that the specific mechanism by which IL-6 influences inflammatory cells may involve the regulation of the IL-6 receptor (IL-6R), the active form of IL-6, and downstream signaling pathways. Notably, there are two receptors for IL-6: IL-6R and gp130. While gp130 is ubiquitously expressed on both immune and non-immune cells, IL-6R expression is restricted to a limited subset of immune cells[35]. The variation in cell surface receptor expression may contribute to the differential regulation of IL-6 levels by various immune cells across different tumor microenvironments. Additionally, the IL-6-related signaling pathway mediated by STAT1 and STAT3 is regarded as a key mechanism for IL-6 function. The Jak-STAT pathway, which is activated through gp130 signaling, is tightly regulated, and

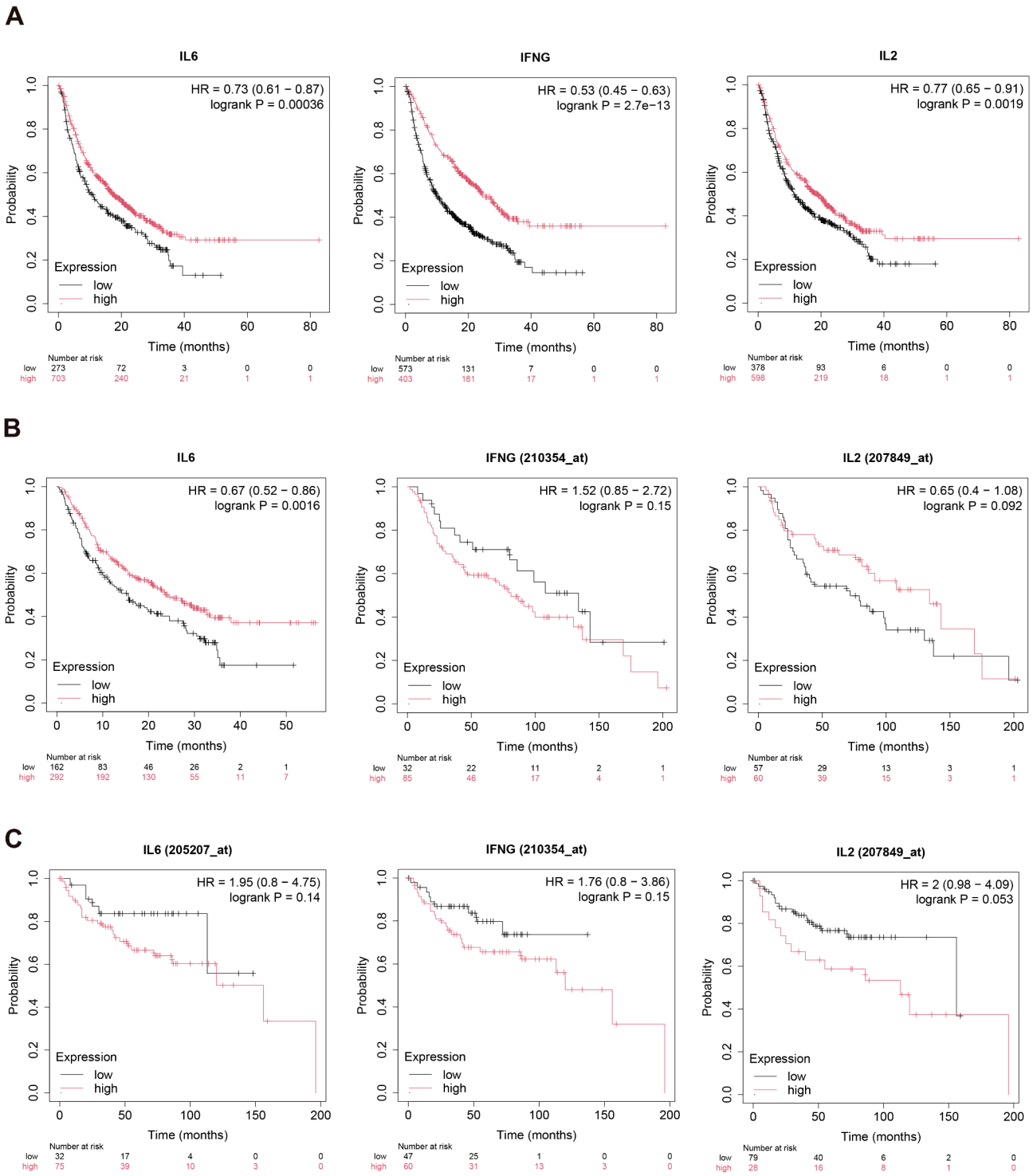

Fig. 7. Cytokine-related survival analysis in CRC patients. (**A**) Cytokine-related survival analysis was conducted in 1061 CRC patients using KM-plotter, focusing on IL6, IFNG, and IL2. (**B**) A total of 602 MSS/MSI-L CRC patients were included in the cytokine-related survival analysis. (**C**) Cytokine-related survival analysis was performed separately for 205 MSI-H CRC patients.

its functional receptor complex requires co-expression of both IL-6 and gp130[36]. The formation of complexes and the stringent activation conditions of the pathway constitute a critical regulatory mechanism in the intricate action of IL-6. Ultimately, TAMs activate the IL-6R/STAT3 pathway in colorectal cancer (CRC) cells, thereby enhancing their proliferation and invasion. Additionally, IL-6 promotes the expression of PD-L1 on the surface of colorectal cancer cells[37,38]. Following the binding of PDL1 to PD1 on inflammatory cells, the functionality of these cells is inhibited. It remains unclear whether this interaction influences cellular infiltration, necessitating

further experimentation in future studies. In addition to the classical mechanism of action, researchers have also discovered that tumor regulation involves the P53/COPS6-related pathway. Notably, the depletion of IL6 levels has been shown to reduce CD8 + T cell infiltration[12,15].

Moreover, we observed that CRC patients with MSS/MSI-L had a more favorable prognosis when exhibiting high levels of IL6 expression. However, in a meta-analysis, researchers suggested that elevated levels of IL6 were associated with poorer prognosis in CRC patients[17]. We propose that potential explanations for the paradoxical prognostic effects of IL-6 may encompass issues related to patient cohorts, the dual nature of IL-6, the active form of IL-6, and the influence of modulation by other cytokines. First, this discrepancy may be attributed to the lack of clear distinction regarding the MSI status of CRC patients in the 10 included studies. Second, given that IL-6 intrinsically possesses dual proinflammatory and anti-inflammatory properties[35], early IL-6 production tends to promote inflammation, while sustained IL-6 levels can subsequently limit inflammatory responses. Consequently, this dual effect may account for contradictory prognostic outcomes. Moreover, the active form of IL-6, which relies on STAT signaling, necessitates the formation of receptor complexes and activation of downstream pathways. The extent to which these biological effects are fully realized at a given concentration may be critical in determining differences in patient prognosis[36]. Finally, in our study, in addition to IL-6 being a pivotal regulator of immune infiltration, both IL-2 and IFN-γ significantly influenced the infiltration of immune cells. These cytokines may exhibit synergistic or antagonistic interactions with IL-6, thereby modulating its role in patient prognosis.

In addition to the effects of IL-6 on inflammatory cells, we observed that the infiltration levels of CD4 + T cells, FOXP3 + Tregs, and M2 macrophages were also influenced by the concentrations of IL-2 and IFN-γ. Notably, IFN-γ emerged as the most influential factor affecting immune infiltration based on our immunohistochemical analysis and correlation studies involving multiple serum cytokines. IFN-γ is considered a key determinant of successful immunotherapy outcomes, similar to IL-6, as it can induce the expression of PD-L1 and enhance the efficacy of immunotherapy[7]. Circulating IFN-γ levels play a critical role in tumor progression. The concentration of serum IFN-γ was correlated with the degree of infiltration by M2 macrophages and CD4 + T cells within the tumor microenvironment. Similarly, researchers have demonstrated that IFN-γ not only counteracts immunosuppression induced by M2 macrophages but also enhances the activity of M1 macrophages[39,40], indicating that IFN-γ may exert dual effects by modulating tumor-associated inflammatory cell infiltration and augmenting inflammatory cell activity. However, survival analysis in MSS CRC patients has not provided conclusive evidence of a direct correlation between IFN-γ levels and patient survival outcomes. We hypothesized that this phenomenon may be attributed to the intricate role of IFNγ in TME. While some studies have indicated an antitumor effect of IFNγ, others have reported opposing findings[40]. The complex mechanisms of action of IFNγ and its involvement in multiple signaling pathways underscore its significance as a cytokine that warrants continued attention. Recombinant IFNγ has been utilized in clinical settings[41]. Given that both IFNγ and IL-6 signal through the JAK/STAT pathway, we propose that, in addition to developing corresponding recombinant agents, potential drugs and targets could be identified from downstream pathways. Furthermore, molecules associated with these downstream pathways may serve as potential biomarkers to guide clinical practice.

Similar to IFNγ, our observations indicate that IL2 plays a role in the infiltration of various inflammatory cells within the tumor microenvironment, including CD4 + T cells, CD8 + T cells, FOXP3 + regulatory T cells, and M2 macrophages. To a significant extent, IL2 also functions as a broad regulator of inflammatory cell infiltration in colorectal cancer[42]. However, IL2 was identified as a core gene, yet no significant difference was observed in survival analysis. One plausible explanation is that IL2 may function as a co-factor in the regulation of IL6 and participate in a signaling pathway loop. The precise mechanism of action remains to be elucidated. Additionally, IL2 may exert broad physiological effects, influencing not only immune regulation but also the nervous, endocrine, and circulatory systems[43,44; 45].Therefore, no direct impact on patient survival has been observed with the combined treatment. However, previous studies have demonstrated that IL2-related biological agents used in the treatment of CRC animal models have achieved certain therapeutic effects. Additionally, an increase in macrophage infiltration following treatment has also been noted[46]. Consequently, there is substantial evidence to suggest that IL2 exerts a considerable influence on immune infiltration. Further investigation is warranted to determine whether IL2 can serve as a potential biomarker for immunotherapy in the future.

Unfortunately, prognostic data for our patient is unavailable at present, and we hope that future studies can address this gap more comprehensively. Similarly, while the relationship between microenvironmental IL6 and CRC development has long been established, further confirmation is required to determine whether this link is related to circulating levels of IL6. Nonetheless, serum IL6 level could potentially serve as one of the reference indicators for guiding clinical medication in immunotherapy.

The occurrence and progression of tumors involve the participation of circulating cytokines. Our study has identified a close correlation between the levels of IL6 and IFNγ in colorectal cancer patients' circulation and immune infiltration, which may explain the limited efficacy of immunotherapy in MSS CRC patients. This association is likely attributed to their involvement in macrophage activation and infiltration within the tumor microenvironment. Consequently, serum cytokine levels could serve as potential indicators for clinical immunotherapy interventions. In the future, combining targeted cytokines with immunotherapy may emerge as a novel treatment option for MSS CRC patients who do not benefit from ICIs.

Materials and methods

Data acquisition and processing

The microarray data for patients with colorectal cancer was primarily obtained from the Gene Expression Omnibus (GEO, https://www.ncbi.nlm.nih.gov/geo/). Three gene expression datasets were selected from GEO, including GSE35279 (from GPL6480), GSE87211 (from GPL13497), and GSE110224 (from GPL570). Among these datasets, GSE35279 included 74 microdissected MSS colorectal tumor samples and 5 microdissected

normal colon epithelium[47]. The GSE87211 dataset comprised of 203 MSS rectal cancer samples and 160 matched mucosal control samples[48], while the GSE110224 dataset consisted of tumor tissue samples and normal colon tissue samples from 17 MSS colorectal adenocarcinoma patients[49]. To further validate the analysis results of this study, we selected the GSE44076 dataset (http://www.colonomics.org/) as an independent validation cohort. This dataset provides gene expression profiles from adjacent normal mucosa and tumor tissues of 98 patients with colorectal adenocarcinoma, thereby offering additional evidence to corroborate our findings.

Differential expression analysis

Batch correction and normalization of the data were conducted using R software (version 4.4.0) and the limma package (version 3.60.4). Initial preprocessing involved removing duplicate gene entries, with averaged expression values for duplicated genes calculated via the avereps function. Quantile analysis was performed to assess the necessity of log transformation; if conditions such as a maximum value exceeding 100 or an interquartile range greater than 50 with the first quartile above zero were met, $\log2(x+1)$ transformation was applied. Data normalization was achieved using the normalizeBetweenArrays function. To ensure consistency, common genes across all files were identified using the Reduce function, and batch types were labeled accordingly. Batch effects were mitigated using the ComBat function from the sva package (version 3.52.0), which constructs surrogate variables to adjust for batch effects in high-dimensional datasets. Principal component analysis (PCA) was performed both before and after batch correction using the ggplot2 (version 3.5.1) and ggpubr (version 0.6.0) packages to visualize changes in data distribution within the reduced dimensionality space, facilitating evaluation of the batch effect removal.

Log-fold change (log2FC) and unadjusted P values were computed for each gene using the limma package. To control the false discovery rate (FDR), the Benjamini-Hochberg method was applied to adjust the P values. Genes with an absolute log2FC greater than 1 and an adjusted P value less than 0.05 were classified as differentially expressed genes (DEGs) between tumor and normal tissues. Furthermore, heatmaps and volcano plots were generated using the pheatmap R package (version 1.0.12) to visually represent the DEGs.

Data acquisition and processing

The weighted gene co-expression network analysis (WGCNA) method was employed to uncover and investigate co-expressed gene modules, with the objective of elucidating the relationship between module genes and clinical phenotypes. Leveraging a combined database, we utilized the R package WGCNA (version 1.72-5) to construct a gene co-expression network for identifying pertinent modules in colorectal cancer. First, genes with expression values that exhibited a standard deviation of less than 0.1 across all samples were excluded. These genes may have stable expression due to measurement errors or other factors and typically lack valuable biological information. Next, the differential gene expression matrix was filtered using the goodSamplesGenes function to remove low-quality samples and genes. Subsequently, a scale-free co-expression network was constructed. The softPower ($\beta = 4$) derived from co-expression similarity was utilized to calculate adjacency, which was then transformed into a topological overlap matrix (TOM) for determining gene connectivity and dissimilarity. Modules were identified through hierarchical clustering and dynamic tree cutting functions. Average linkage hierarchical clustering was employed to group genes with similar expression profiles into modules, while TOM-based dissimilarity measure and gene dendrogram required a minimum genome size of 60. By evaluating the degree of difference among characteristic genes within each module, a threshold of 0.25 was set to select cut lines in the module dendrogram for merging several modules together for further analysis. The resulting characteristic gene network was visualized accordingly. Integrating the clustering tree branches with clinical phenotype data, comprehensive evaluations utilizing gene significance (GS) and module membership (MM) were conducted to accurately identify core modules closely associated with clinical features. Finally, we obtained 19 co-expression modules.

Key genes screening and GO and KEGG enrichment analyses

The intersection between differentially expressed genes (DEGs) and key genes identified by weighted gene co-expression network analysis (WGCNA) was determined using the VennDiagram package (version 1.6.0) in R, resulting in the identification of 1301 candidate key genes. Gene ontology (GO) and Kyoto Encyclopedia of Genes and Genomes (KEGG) enrichment analyses were performed using the ClusterProfiler package (version 4.12.0) in R, with a significance threshold set at $P < 0.05$, to explore the potential functions and pathways associated with these genes.

Construction of protein-protein interaction networks(PPI)

We utilized the STRING online tool (https://string-db.org/) to import the aforementioned intersection genes and validate the organism as "Homo sapiens". The minimum interaction score was set to the highest confidence level (0.9), and disconnected nodes were hidden. Subsequently, Cytoscape 3.9.0 software was employed for visualizing the protein-protein interaction (PPI) network, while cytoHubba plug-in calculated the degree values of nodes. In this study, core genes in the PPI network were identified as targets with degree values surpassing the median value. The genes were ranked based on their degree values, highlighting the top ten key genes.

Construction of the receiver operating characteristic (ROC)

Hub genes were further validated using receiver operating characteristic (ROC) curve analysis to assess the diagnostic value of differentially expressed genes (DEGs). The area under the curve (AUC), sensitivity, and 1-specificity were calculated using the R package pROC (version 1.18.5). AUC values in the ranges of 0.5–0.7, 0.7–0.9, and >0.9 were classified as indicative of low, moderate, and high accuracy, respectively. Sensitivity and 1-specificity were jointly evaluated to determine the model's validity; a value closer to 1.0 for both metrics

indicates higher validity. Additionally, we employed nomograms, a statistical prediction tool, to construct models predicting disease risk based on hub gene expression levels. In constructing logistic regression models, L2 regularization (also known as Ridge regression) was incorporated to control model complexity by penalizing large coefficients, thereby mitigating overfitting risks. The strength of regularization was adjusted via the penalty parameter. Finally, the rms package was utilized to calibrate the regression model, and a calibration curve was generated to evaluate the model's predictive accuracy.

Immune infiltration analysis

To evaluate the abundance of immune infiltrates, we utilized integrated and standardized gene-expression profiling data to identify various types of immune cells within tissues. Specifically, we employed the default reference signature matrix provided by the CIBERSORT algorithm, which encompasses gene expression signatures for 22 human immune cell subsets. The analysis was conducted using the CIBERSORT package in R software, with the number of permutations set to 1000 and a significance level of 0.05. The resulting immune cell infiltration matrix generated by the CIBERSORT algorithm details the relative proportions of the 22 immune cell types in each sample. To visualize these proportions across different samples, we used the pheatmap package (version 1.0.12) to generate heat maps. Additionally, the corrplot package (version 0.94) was utilized to create correlation heat maps illustrating the relationships between different immune cells. Differences in immune-cell infiltration between the tumor and control groups were depicted using violin plots generated by the vioplot package (version 0.5.0). Furthermore, we explored the potential correlations between the expression levels of key genes (IL-6, IFNG, and IL-2) and the patterns of immune cell infiltration. Spearman correlation analysis was performed to assess the relationship between gene expression and immune cell enrichment, with results visualized using a lollipop plot. Through these comprehensive steps, we thoroughly evaluated and visualized the extent of immune cell infiltration in both tumor and normal samples, providing valuable insights into the immune microenvironment of colorectal cancer (CRC).

Patients' specimens and clinical data collection

A total of 55 CRC tissues and corresponding adjacent normal tissues were collected from First Affiliated Hospital of Chongqing Medical University. Primary tumors located at the cecum, ascending colon, and transverse colon were defined as right side, whereas primary tumors located at the splenic flexure, descending colon and sigmoid colon were defined as left side. Patient characteristics including age at diagnosis, gender, common serum cytokines(IL2,IL4,IL6,IL10,IL17,TNFα and IFNγ), tumor location, histological type, tumor grade, tumor stage, chemotherapy history, K-RAS status, and mismatch repair (MMR) status were collected from patient records. The patient's serum cytokines, including IL-2, IL-4, IL-6, IL-10 and IL-17, were quantified using flow cytometry (Roche Diagnostics Cobas 80-E602) with antibodies supplied by Jiangxi Sakey Biotechnology Co., Ltd. which is no dilution required. The samples were incubated at room temperature in the dark for 2.5 to 3 h. The sensitivity levels for IL-17 A, IL-2, IL-4, and IL-6 were 10 pg/mL, while that for IL-10 was 2.5 pg/mL. All methods used in the study were conducted in accordance with the approved guidelines. Ethics approval and consent were obtaining from clinical patients. The study protocol was approved by Medical Research Ethics Review Committee of the First Affiliated Hospital of Chongqing Medical University (2024-190-01).

Immunohistochemistry (IHC)

Immunohistochemistry (IHC) assay the tissue specimens of the 55 MSS CRC patients were fixed with formalin, paraffin-embedded and sliced into 3 mm sections. After de-paraffinization in xylene and dehydration in ethanol, the sections were incubated with 0.3% hydrogen peroxide methanol for 10 min to eliminate endogenous peroxidase. Monoclonal antibody anti-human CD3, CD4, CD8, CD163(purchased from MXB biotechnologies, Fujian, China and no dilution required) were added and incubated overnight at 4 C in a refrigerator. After being rinsed with PBS, Rabbit Anti-Human IgG H&L and Rabbit Anti-Mouse IgG H&L (Beijing Zhongshan Jinqiao Biotechnology Co., Ltd., Beijing, China) was added dropwise, incubated at room temperature for 20 min, rinsed with PBS, DAB color developed for 3 min, hematoxylin counterstained, dehydrated, hyalinized with xylene, and sealed with neutral gum. KFBIO digital pathology slide scanner(KF-PRO-020-HI) was used for panoramic scanning and information storage. The results were interpreted by calculating the degree of staining infiltration of specific immune cells by Image J pro.

Statistical analysis

All data analysis in our study were performed using GraphPad Prism 9.5(GraphPad, USA) and SPSS 18.0(SPSS, USA) software. Mann Whitney test was performed comparing two groups. For multiple comparisons, nonparametric one-way ANOVA was performed using the Kruskal Wallis (KW) test. All tests were two- tailed. The association between the KRAS mutation and the clinical characters was assessed with the Spearman correlation coefficient. Quantitative data are presented as the mean ± SD or percentage. Differences were considered to be significant at p values < 0.05.

Data availability

The original data included in the figures are shown in the article. For further inquiries, please contact the corresponding author.

Received: 21 November 2024; Accepted: 3 March 2025
Published online: 13 March 2025

References

1. Akbar, S. et al. Circulating exosomal immuno-oncological checkpoints and cytokines are potential biomarkers to monitor tumor response to anti-PD-1/PD-L1 therapy in non-small cell lung cancer patients. *Front. Immunol.* **13** https://doi.org/10.3389/fimmu.2022.1097117 (2023).
2. DT, L. et al. Mismatch repair deficiency predicts response of solid tumors to PD-1 blockade. *Science* **357** (6349), 409–413 (2017).
3. Ganesh, K. Optimizing immunotherapy for colorectal cancer. *Nat. Rev. Gastroenterol. Hepatol.* **19** (2), 93–94. https://doi.org/10.1038/s41575-021-00569-4 (2021).
4. Ganesh, K. et al. Immunotherapy in colorectal cancer: rationale, challenges and potential. *Nat. Rev. Gastroenterol. Hepatol.* **16** (6), 361–375. https://doi.org/10.1038/s41575-019-0126-x (2019).
5. Overman, M. J. et al. Nivolumab in patients with metastatic DNA mismatch repair-deficient or microsatellite instability-high colorectal cancer (CheckMate 142): an open-label, multicentre, phase 2 study. *Lancet Oncol.* **18** (9), 1182–1191. https://doi.org/10.1016/s1470-2045(17)30422-9 (2017).
6. Al Zein, M. et al. Immunotherapy and immunoevasion of colorectal cancer. *Drug Discov. Today* **28** (9). https://doi.org/10.1016/j.drudis.2023.103669 (2023).
7. Lin, A. et al. Crosstalk between the MSI status and tumor microenvironment in colorectal cancer. *Front. Immunol.* **11** https://doi.org/10.3389/fimmu.2020.02039 (2020).
8. Yang, C. et al. Improving the efficiency of immune checkpoint inhibitors for metastatic pMMR/MSS colorectal cancer: Options and strategies. *Crit. Rev. Oncol. Hematol.* **200** https://doi.org/10.1016/j.critrevonc.2023.104204 (2024).
9. Zhang, D. et al. ASCL2 induces an immune excluded microenvironment by activating cancer-associated fibroblasts in microsatellite stable colorectal cancer. *Oncogene* **42** (38), 2841–2853. https://doi.org/10.1038/s41388-023-02806-3 (2023).
10. Chen, S. et al. YY1 complex in M2 macrophage promotes prostate cancer progression by upregulating IL-6. *J. Immunother. Cancer* **11** (4). https://doi.org/10.1136/jitc-2022-006020 (2023).
11. Hidalgo-García, L. et al. Administration of intestinal mesenchymal stromal cells reduces colitis-associated cancer in C57BL/6J mice modulating the immune response and gut dysbiosis. *Pharmacol. Res.* 195. https://doi.org/10.1016/j.phrs.2023.106891 (2023).
12. Pedersen, L. et al. Voluntary running suppresses tumor growth through Epinephrine- and IL-6-Dependent NK cell mobilization and redistribution. *Cell Metabol.* **23** (3), 554–562. https://doi.org/10.1016/j.cmet.2016.01.011 (2016).
13. Wei, C. et al. Crosstalk between cancer cells and tumor associated macrophages is required for mesenchymal circulating tumor cell-mediated colorectal cancer metastasis. *Mol. Cancer* **18** (1). https://doi.org/10.1186/s12943-019-0976-4 (2019).
14. Picard, E. et al. Relationships between immune landscapes, genetic subtypes and responses to immunotherapy in colorectal cancer. *Front. Immunol.* **11** https://doi.org/10.3389/fimmu.2020.00369 (2020).
15. Wei, X., Zhang, J. Y., Feng, X., Zhou, S. & B Neoadjuvant three-dimensional conformal radiotherapy for resectable hepatocellular carcinoma with portal vein tumor thrombus A randomized, open-label, multicenter controlled study. *J. Clin. Oncol.* **37** (24), 2141–2151. https://doi.org/10.1200/JCO.18 (2019).
16. Chen, I. M. et al. Prognostic value of combined detection of serum IL6, YKL-40, and C-reactive protein in patients with unresectable pancreatic Cancer. *Cancer Epidemiol. Biomark. Prev.* **29** (1), 176–184. https://doi.org/10.1158/1055-9965.Epi-19-0672 (2020).
17. Xu, J. et al. Diagnostic and prognostic value of serum Interleukin-6 in colorectal cancer. *Medicine* **95** (2). https://doi.org/10.1097/md.0000000000002502 (2016).
18. Talaat, R. M. et al. CD38 and Interleukin 6 gene polymorphism in Egyptians with diffuse large B-Cell lymphoma (DLBCL). *Immunol. Investig.* **44** (3), 265–278. https://doi.org/10.3109/08820139.2014.989328 (2015).
19. Kanehisa, M. Toward understanding the origin and evolution of cellular organisms. *Protein Sci.* **28** (11), 1947–1951. https://doi.org/10.1002/pro.3715 (2019).
20. Kanehisa, M. et al. KEGG: biological systems database as a model of the real world. *Nucleic Acids Res.* **53** (D1). https://doi.org/10.1093/nar/gkae909 (2025). D672-D677.
21. M, K. & S., G KEGG: Kyoto encyclopedia of genes and genomes. *Nucleic Acids Res.* **28** (1), 27–30. https://doi.org/10.1093/nar/28.1.27 (2000).
22. Cheng, C. C. et al. Sorafenib suppresses radioresistance and synergizes radiotherapy-mediated CD8 + T cell activation to eradicate hepatocellular carcinoma. *Int. Immunopharmacol.* **112** https://doi.org/10.1016/j.intimp.2022.109110 (2022).
23. Propper, D. J. & Balkwill, F. R. Harnessing cytokines and chemokines for cancer therapy. *Nat. Reviews Clin. Oncol.* **19** (4), 237–253. https://doi.org/10.1038/s41571-021-00588-9 (2022).
24. Huseni, M. A. et al. CD8 + T cell-intrinsic IL-6 signaling promotes resistance to anti-PD-L1 immunotherapy. *Cell. Rep. Med.* **4** (1). https://doi.org/10.1016/j.xcrm.2022.100878 (2023).
25. Hailemichael, Y. et al. Interleukin-6 Blockade abrogates immunotherapy toxicity and promotes tumor immunity. *Cancer Cell.* **40** (5), 509–523e506. https://doi.org/10.1016/j.ccell.2022.04.004 (2022).
26. Atreya, R. & N. M Involvement of IL-6 in the pathogenesis of inflammatory. *Clin. Rev. Allergy Immunol.* **28** (3), 187–196. https://doi.org/10.1385/CRIAI:28:3:187 (2005).
27. De Simone, V. et al. Th17-type cytokines, IL-6 and TNF-α synergistically activate STAT3 and NF-kB to promote colorectal cancer cell growth. *Oncogene* **34** (27), 3493–3503. https://doi.org/10.1038/onc.2014.286 (2014).
28. Yao, X. et al. Targeting interleukin-6 in inflammatory autoimmune diseases and cancers. *Pharmacol. Ther.* **141** (2), 125–139. https://doi.org/10.1016/j.pharmthera.2013.09.004 (2014).
29. Hu, F. et al. IL-6 regulates autophagy and chemotherapy resistance by promoting BECN1 phosphorylation. *Nat. Commun.* **12** (1). https://doi.org/10.1038/s41467-021-23923-1 (2021).
30. Zhao, S. et al. Highly-metastatic colorectal cancer cell released miR-181a-5p-rich extracellular vesicles promote liver metastasis by activating hepatic stellate cells and remodelling the tumour microenvironment. *J. Extracell. Vesicles* **11** (1). https://doi.org/10.1002/jev2.12186 (2022).
31. Knüpfer, H. & Preiss, R. Serum interleukin-6 levels in colorectal cancer patients—A summary of published results. *Int. J. Colorectal Dis.* **25** (2), 135–140. https://doi.org/10.1007/s00384-009-0818-8 (2009).
32. Cozen, W. IL-6 levels and genotype are associated with risk of young adult hodgkin lymphoma. *Blood* **103** (8), 3216–3221. https://doi.org/10.1182/blood-2003-08-2860 (2004).
33. Li, Y. et al. Disease-related expression of the IL6/STAT3/SOCS3 signalling pathway in ulcerative colitis and ulcerative colitis-related carcinogenesis. *Gut* **59** (2), 227–235. https://doi.org/10.1136/gut.2009.184176 (2010).
34. Li, Y. et al. Nicotinamide N-methyltransferase promotes M2 macrophage polarization by IL6 and MDSC conversion by GM-CSF in gallbladder carcinoma. *Hepatology* https://doi.org/10.1097/hep.0000000000000028 (2023).
35. Hunter, C. A. & Jones, S. A. IL-6 as a keystone cytokine in health and disease. *Nat. Immunol.* **16** (5), 448–457. https://doi.org/10.1038/ni.3153 (2015).
36. Schmidt-Arras, D. & Rose-John, S. IL-6 pathway in the liver: from physiopathology to therapy. *J. Hepatol.* **64** (6), 1403–1415. https://doi.org/10.1016/j.jhep.2016.02.004 (2016).
37. Lamano, J. B. et al. Glioblastoma-Derived IL6 induces immunosuppressive peripheral myeloid cell PD-L1 and promotes tumor growth. *Clin. Cancer Res.* **25** (12), 3643–3657. https://doi.org/10.1158/1078-0432.Ccr-18-2402 (2019).
38. Niu, Y. The effect and mechanism of inflammatory cytokine IL6 in promoting PD-L1 expression in colorectal cancer cells. *Chin. J. Pathophysiol.* (2020).
39. Hatzioannou, A. et al. An intrinsic role of IL-33 in treg cell–mediated tumor immunoevasion. *Nat. Immunol.* **21** (1), 75–85. https://doi.org/10.1038/s41590-019-0555-2 (2019).

40. Jorgovanovic, D. et al. Roles of IFN-γ in tumor progression and regression: a review. *Biomark. Res.* **8** (1). https://doi.org/10.1186/s40364-020-00228-x (2020).
41. Windbichler, G. H. & Hausmaninger, H. Interferon-gamma in the first-line therapy of ovarian cancer: a randomized phase III trial. *Br. J. Cancer* **82** (6), 1138–1144. https://doi.org/10.1054/bjoc.1999.1053 (2000).
42. Krastev, Z. et al. Non-melanoma and non-renal cell carcinoma malignancies treated with interleukin-2. *Hepatogastroenterology* **50** (52), 1006–1016 (2003).
43. Das, U. N. Beneficial effect(s) of n-3 fatty acids in cardiovascular diseases: but, why and how? *Prostaglandins Leukotrienes Essent. Fat. Acids (PLEFA)* **63** (6), 351–362. https://doi.org/10.1054/plef.2000.0226 (2000).
44. Roya, E. B & Kevinl, B. Immunological responses to injury and grafting in the central nervous system of nonhuman primates. *Cell Transplant.* **7**, 109–120. https://doi.org/10.1177/096368979800700206 (1998).
45. Vial, T. & J Descotes clinical toxicity of interleukin-2. *Drug Saf.* **7** (6), 417–433. https://doi.org/10.2165/00002018-199207060-00004 (1992).
46. Kusnierczyk, H. et al. Further development of local IL-2 therapy of cancer: multiple versus single IL-2 treatment of transplanted murine colon carcinoma. *Cancer Immunol. Immunother.* **53** (5), 445–452. https://doi.org/10.1007/s00262-003-0490-8 (2004).
47. Lee, J. W. et al. Cell cycle-dependent rho GTPase activity dynamically regulates cancer cell motility and invasion in vivo. *PLoS One* **8** (12). https://doi.org/10.1371/journal.pone.0083629 (2013).
48. Hu, Y. et al. Colorectal cancer susceptibility loci as predictive markers of rectal cancer prognosis after surgery. *Genes Chromosom. Cancer* **57** (3), 140–149. https://doi.org/10.1002/gcc.22512 (2017).
49. Vlachavas, E. I. et al. Radiogenomic analysis of F-18-fluorodeoxyglucose positron emission tomography and gene expression data elucidates the epidemiological complexity of colorectal cancer landscape. *Comput. Struct. Biotechnol. J.* **17**, 177–185. https://doi.org/10.1016/j.csbj.2019.01.007 (2019).

Acknowledgements

We extend our gratitude to all participants in this hearing research.

Author contributions

YT designed the experiments; Clinical data collection was managed by QSL, MX, ML; JH, SYJS were responsible for the process of IHC experiments. RX and JH analysis of the result; review and editing were completed by YT and JH; YT, WWL and YYY was responsible for funding acquisition and manuscript modification. All authors have read and agreed to the published version of the manuscript.

Declarations

Competing interests

The authors declare no competing interests.

Ethics declarations

The study was conducted according to the guidelines of the Declaration of Helsinki, and approved by Medical Research Ethics Review Committee of the First Affiliated Hospital of Chongqing Medical University On September 23, 2024(2024-190-01).

Additional information

Supplementary Information The online version contains supplementary material available at https://doi.org/10.1038/s41598-025-92817-9.

Correspondence and requests for materials should be addressed to W.L. or Y.T.